

# Influence of experimental temperature and duration of laboratory confined thermal maturation experiments on the evolution of the porosity of organic-rich source rocks

Amélie Cavelan, Mohammed Boussafir, Claude Le Milbeau, Sandrine Delpeux, Fatima Laggoun-Défarge

▶ **To cite this version:**

Amélie Cavelan, Mohammed Boussafir, Claude Le Milbeau, Sandrine Delpeux, Fatima Laggoun-Défarge. Influence of experimental temperature and duration of laboratory confined thermal maturation experiments on the evolution of the porosity of organic-rich source rocks. Marine and Petroleum Geology, 2020, 122, pp.104667. 10.1016/j.marpetgeo.2020.104667 . insu-02918247

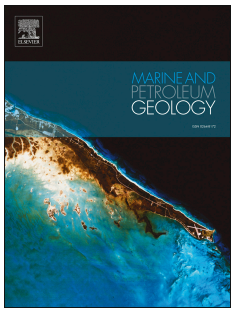
**HAL Id: insu-02918247**
**https://insu.hal.science/insu-02918247**

Submitted on 20 Aug 2020

**HAL** is a multi-disciplinary open access archive for the deposit and dissemination of scientific research documents, whether they are published or not. The documents may come from teaching and research institutions in France or abroad, or from public or private research centers.

L'archive ouverte pluridisciplinaire **HAL**, est destinée au dépôt et à la diffusion de documents scientifiques de niveau recherche, publiés ou non, émanant des établissements d'enseignement et de recherche français ou étrangers, des laboratoires publics ou privés.

# Journal Pre-proof




Influence of experimental temperature and duration of laboratory confined thermal maturation experiments on the evolution of the porosity of organic-rich source rocks

Amélie Cavelan, Mohammed Boussafir, Claude Le Milbeau, Sandrine Delpeux, Fatima Laggoun-Défarge

PII: S0264-8172(20)30450-5

DOI: https://doi.org/10.1016/j.marpetgeo.2020.104667

Reference: JMPG 104667

To appear in: *Marine and Petroleum Geology*

Received Date: 9 June 2020

Revised Date: 22 July 2020

Accepted Date: 18 August 2020

Please cite this article as: Cavelan, Amé., Boussafir, M., Le Milbeau, C., Delpeux, S., Laggoun-Défarge, F., Influence of experimental temperature and duration of laboratory confined thermal maturation experiments on the evolution of the porosity of organic-rich source rocks, *Marine and Petroleum Geology* (2020), doi: https://doi.org/10.1016/j.marpetgeo.2020.104667.

This is a PDF file of an article that has undergone enhancements after acceptance, such as the addition of a cover page and metadata, and formatting for readability, but it is not yet the definitive version of record. This version will undergo additional copyediting, typesetting and review before it is published in its final form, but we are providing this version to give early visibility of the article. Please note that, during the production process, errors may be discovered which could affect the content, and all legal disclaimers that apply to the journal pertain.

© 2020 Published by Elsevier Ltd.

Journal Pre-proof

**Sample CRediT author statement**

**Amelie Cavelan** : Investigation - Original draft preparation- Redaction - Writing - Review & Editing. **Mohammed Boussafir** : Conceptualization - Redaction -Supervision- Review & Editing - Funding acquisition. **Claude Le Milbeau** : Methodology – Validation – Reviewing. **Sandrine Delpeux** : Methodology – Validation – Reviewing. **Fatima Laggoun-Défarge** : Supervision – Project administration – Conceptualization .

Journal Pre-proof

Journal Pre-proof

# Influence of experimental temperature and duration of laboratory confined thermal maturation experiments on the evolution of the porosity of organic-rich source rocks.

Amélie Cavelan[a,b*], Mohammed Boussafir[a], Claude Le Milbeau[a], Sandrine Delpeux[c], Fatima Laggoun-Défarge[a].

(a) Université d'Orléans, CNRS, BRGM, ISTO, UMR 7327, F-45071, Orléans, France

(b) Université de Lorraine, CNRS, LIEC, F-54000, Nancy, France

(c) CNRS, ICMN, UMR7374, F-45071, France

*Corresponding author: amelie.cavelan@univ-lorraine.fr

**Abstract:** To investigate the influence of the duration-temperature pairs chosen for laboratory thermal maturations on the evolution of the organic matter (OM) and porosity of the clay-rich source rocks with increasing maturity, long duration (104 days) thermal maturations, bulk, molecular geochemical OM characterization (Rock Eval, GC-TCD, GC/MS) and nitrogen adsorption porosimetry were applied on six type II mudstones from the Kimmeridge Clay formation. These results were compared with shorter duration experiments (72 hours) previously carried out. The results show that the increase in the duration of thermal maturation experiments enhanced the degradation of heavy polar OM components into saturated and aromatic hydrocarbons, leading to the production of similar amounts of extractible OM (EOM) enriched in saturated and aromatic hydrocarbons. Then, in preventing the early breaking of low energy bonds, the lower temperature used for the longer duration experiments led to a less pronounced early cracking of OM resulting in a different timing of gas generation. This process did not influence the general evolution of the pore volume, which increased during gas generation. Whatever the duration-temperature pair chosen for maturation experiments highly oil-prone samples formed lower pore volumes during gas generation. Increasing the duration of thermal maturation seemed, nevertheless, to influence the amplitude and the timing of pore alteration events that occur during gas generation, leading to slightly different pore size distributions and pore volumes between

Journal Pre-proof

short and long duration experiments. However, these differences remain limited, suggesting that results from different time-duration experiments can be easily compared.

**Key words:** thermal maturation; porosity; source rocks; nitrogen adsorption; GC-MS

## Introduction

The growing interest for unconventional resources has led to a considerable shift in the approach to characterize these reservoirs. The use of a combination of various cutting-edge technologies to quantify and image the complex structure of these fined-grained rocks has allowed a more precise understanding of the evolution of their porosity. The interparticle porosity associated with the mineral matrix generally decreases during burial, filled by entrapped EOM or reduced by compaction and OM ductile deformations (DiStefano et al., 2016; Furmann et al., 2016; Guo et al., 2018; Han et al., 2017; Katz and Arango, 2018; Loucks et al., 2009; Modica and Lapierre, 2012; X. Wang et al., 2020; Wang et al., 2019). Conversely, the progressive conversion of OM, the carbon loss and the significant variations of volume, which occur during oil and gas generation result in the growth of a secondary OM-hosted porosity (Bernard et al., 2012a; Chalmers and Bustin, 2008; Chen and Xiao, 2014; Curtis et al., 2012; Han et al., 2017; Jarvie et al., 2007; Ko et al., 2016, 2018; Loucks et al., 2012; X. Wang et al., 2020; Wu et al., 2019). In the vast majority of thermally mature rocks, the OM is the main contributor to the porosity (Bernard et al., 2012a; Cavelan et al., 2019a; Chalmers et al., 2012; Han et al., 2019; Juliao et al., 2015; Katz and Arango, 2018; Ko et al., 2018; Kuila et al., 2014; Loucks et al., 2009, 2012; Milliken et al., 2013; Pan et al., 2015). Thermal maturity and the initial OM composition, which controlled the amount of oil and gas generated during maturation, are thus widely considered as the key factors controlling the formation and the development of pores in organic-rich source rocks (Bernard et al., 2012a, 2012b; Cavelan et al., 2019a, 2020; Chalmers and Bustin, 2008; Chen and Xiao, 2014; Curtis et al., 2012; Ko et al., 2018; Loucks et al., 2009).

To investigate the relation between thermal maturity, OM composition and pore evolution, the use of laboratory thermal maturation has become more common these last years (Cavelan et al., 2019a, 2020; Chen and Xiao, 2014; Guo et al., 2017; Hu et al., 2015; Ko et al., 2016, 2018; X. Wang et al.,

Journal Pre-proof

2020; Y. Wang et al., 2020; Zhang et al., 2013). As demonstrated by these previous works, the use of laboratory thermal maturations could be a key method to obtain rocks of various maturities from the same initial material. However, various duration-temperature pairs can be selected for these experiments. While the effects of laboratory thermal maturation conditions on OM thermal degradation processes have been well studied (Behar et al., 2003; Landais et al., 1994; Michels et al., 1995, 1992), the effects on the evolution and the development of porosity have never been assessed. As OM thermal degradation processes are governed by the first order Arrhenius law, a plethora of many duration-temperature pairs should be able to be used to reach the same stage of maturity (Landais et al., 1994; Wood, 1988). However, previous studies show that the experimental temperature and duration of these laboratory simulations are not really exchangeable parameters (Landais et al., 1994), as increasing the thermal maturation duration and lowering the experimental temperatures could significantly influence the yield, the composition and the timing at which liquid and gaseous hydrocarbons are generated. In view of the strong relation existing between organic-rich source rocks porosity, OM thermal degradation processes, and oil and gas generation, these differences may influence the formation and the development of pores with increasing maturity. It seemed interesting therefore to test how the differences observed between short- and long-duration experiments can influence the formation and the development of organic-rich source rocks porosity. This may help to assess whether artificial maturation can accurately simulate the porosity evolution of natural source rocks.

To this end, long duration (104 days) gold-tube anhydrous confined thermal maturation experiments were carried out on six immature organic-rich source rocks from the Kimmeridge Clay formation. The concomitant evolutions of the bulk, molecular organic geochemistry and porosity during maturation were determined using Rock Eval® pyrolysis, GC-TCD, GC/MS and nitrogen adsorption measurements. The results were then compared with the shorter duration experiments (72 hours) previously carried out (Cavelan et al., 2019a, 2020). The present study aimed particularly to better understand the relation between the duration-temperature pair of anhydrous confined thermal maturation and the ability of rocks to develop and preserve pores with increasing maturity.

## 1. Samples and methods

### 1.1. Geological background

The late Jurassic Kimmeridge clay formation (KCF) consists of organic-rich marine shales deposited from the Kimmeridgian to the Tithonian (Herbin et al., 1995; Rawson and Riley, 1982). Onshore, this formation outcrops across England from the Dorset to the north Yorkshire; offshore the KCF is largely distributed throughout the Northern, Central and Southern North Sea (Fig. 1, Rawson and Riley, 1982).

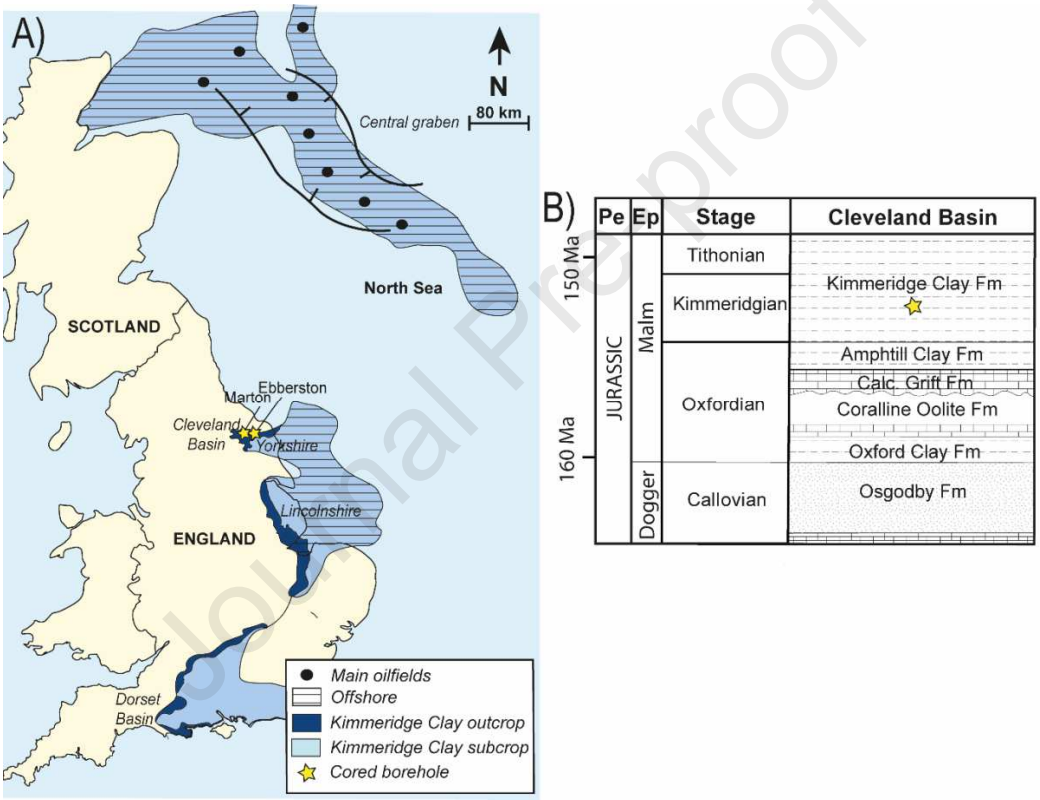



Fig. 1. A) Kimmeridge clay formation across England and North Sea; location of the studies boreholes (modified from Gallois, 2004). B) Simplified stratigraphic column of the Cleveland Basin (modified from Powell, 2010).

For this study, six immature KCF mudstones (Vitrinite reflectance ca. 0.42%, Cavelan et al., 2020) were selected from Marton and Ebberston boreholes between 69.98 and 128.78 m deep (Yorkshire, UK, Fig.1). The organic geochemistry, the mineralogy and the porosity of this geological section were well-documented in the past twenty years (Boussafir et al., 1995a, 1995b; Boussafir and Lallier-Vergès, 1997; Cavelan et al., 2020; Desprairies et al., 1995; Ramanampisoa and Disnar, 1994;

Journal Pre-proof

Ramanampisoa and Radke, 1995). The studied rocks consist in finely laminated marine argillaceous mudstones with total organic carbon ranges between 3 to 15.4 wt.% (Rock Eval® 6 TOC) and a high OM oil generation potential varying between 418 to 617 mg of HC/g of TOC (Rock Eval® 6 hydrogen index, Cavelan et al., 2019b). The OM is mainly composed of amorphous organic matter (AOM) including in the order of decreasing abundance: highly oil-prone phytoplanktonic orange AOM, algal brown AOM and black AOM. This OM is accompanied by a minor contribution of structured components derived from zooplankton (pores, pollens,…) and plant tissues (Boussafir et al., 1995b; Boussafir and Lallier-Vergès, 1997).

### 1.2. Bulk and molecular OM composition

The devices used for anhydrous confined thermal maturation experiments were described in Cavelan et al. (2019a). About 1g of each sample was crushed into powder (particle size: 250 µm to 180 µm), loaded into gold cells (dia: 0.50 mm, len: 6,5 cm) and introduced into high-pressure stainless-steel autoclaves pressurized with water. A constant confining external pressure was maintained at 600 bar during the experiments. Samples were isothermally heated at 283, 338 and 390°C for 104 days in order to obtain the three ranks of maturity previously reached by the short-duration experiments of Cavelan et al., (2019a): the early oil generation, the condensate wet gas zone and the dry gas zone (Fig.2). The increasing rate of the temperature used for the experiments may impact thermal maturation results. To avoid any effect other than the experimental temperature and duration of the experiments on the results, the same temperature increasing rate was used for the long and short-duration experiments as well as for each stage of maturity: 5.5°C.min$^{-1}$. At the end of the experiments, the oven was turned off and the autoclaves were slowly depressurized. After maturation, the gold cells were sealed in separate 25 cm$^3$- glass bottles and pierced under vacuum. Approximate 2 cm$^3$ of gases were sampled using a gas tight syringe and injected into a gas chromatography coupled with a thermal conductivity detector (GC-TCD). Gas composition was determined using a Perkin Elmer® Clarus 580 gas chromatograph (Supelco® Carboxen 1010 Plot® Capillary column: 30 m × 0.53 mm i.d., 0.15 µm film thickness) using the same operating conditions described in Cavelan et al. (2019a). Individual gas components were identified by comparison with the relative retention times of

standard. Each gas content was quantified using its respective peak surface area and calibration curves by assuming ideal gas behavior.

Between 50 and 60 mg of dried and powdered samples were analyzed using a Rock-Eval® 6 pyrolizer (Vinci Technologies, Rueil Malmaison). For the pyrolysis, samples were first isothermally heated for 2 min at 200°C under helium atmosphere. The oven temperature was then raised with a ramp of 30°C.min$^{-1}$ to 650°C and held for 3 min. For the oxidation, samples were isothermally heated under purified air at 400°C. The temperature was then raised to 850°C at 30°C.min$^{-1}$ and held 5 min. The parameters used in this study are the TOC (wt. %), the hydrogen index (HI, mgHC/g TOC) and the oxygen index (OI, mgCO2/g TOC). The significance of these parameters was described by Espitalie et al. (1985a, b) and Lafargue et al. (1998).

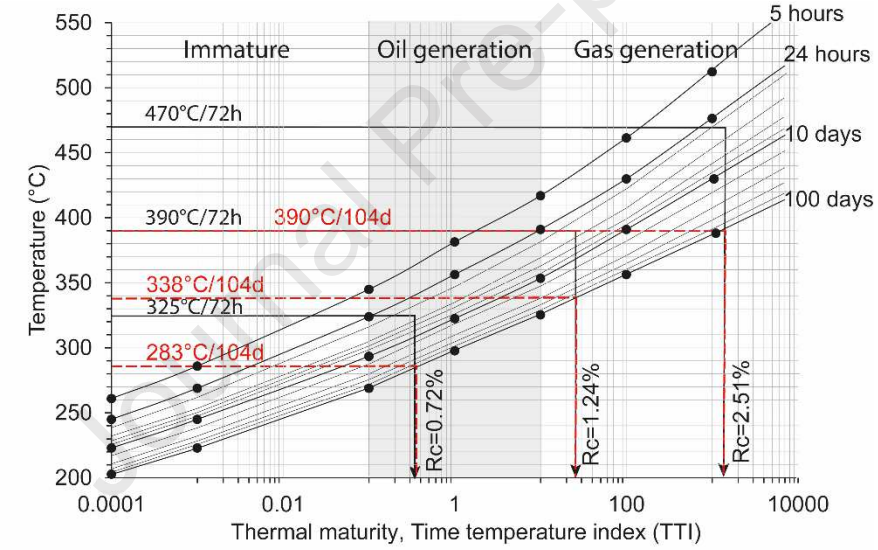



Fig. 2. Relation between maturity, temperature and duration of thermal maturations. In red: long-duration experiments (this study). In black: short-duration experiments and calculated vitrinite reflectance from Cavelan et al., (2019a). This chart was drawn from the data of Landais et al. (1994).

About 1g of powdered samples was then extracted with a solution of dichloromethane/methanol (1/1) using ultrasonication (10 min). The total extractible OM (EOM) was recovered by centrifugation, dried under nitrogen, weighed and desulfurized with copper shavings. The EOM was separated using deactivated silica gel (5% with water) chromatography column. The saturated hydrocarbons (SAT) were recovered by elution with heptane. The aromatic hydrocarbons

Journal Pre-proof

(ARO) were recovered by the subsequent elution of a mixture of heptane/toluene (3/1) and (2/2). The polar hydrocarbons were recovered by methanol elution. Each dried fraction was weighed. Asphaltenes remain trapped in the chromatography columns. The mass of asphaltenes was thus determined by difference in mass between the mass of the total EOM extract and the mass of the recovered fractions (SAT+ARO and polar). Some polar compounds (resins) can be trapped with asphaltenes in the columns. The mass of asphaltenes was thus counted with the mass of polar hydrocarbons to obtain the total mass of the NSO fraction. SAT and ARO were analyzed by gas chromatography-mass spectrometry (GC-MS) using a Trace-GC Ultra gas chromatograph equipped with a Thermo Trace-Gold 5 MS capillary column (60 m × 0.25 mm i.d, 0.25 film thickness) and coupled to a TSQ Quantum XLS mass spectrometer (MS). The apparatus was fitted with an AS 3000 auto sampler (Thermo Scientific). The operating conditions were described in Cavelan et al., (2019a). The identification of each molecule presents in the SAT and ARO fractions was done by comparing retention times and mass spectra with previously published data. Their quantification was based on the integration of their peak area. Squalane was used as internal standard.

### 1.3. Pore volume, specific surface area and pore size distribution

The pore volume, the specific surface area and the pore size distribution (PSD) were determined by low-pressure nitrogen adsorption on a Micromeritics® ASAP -2420 apparatus. Before analysis, the samples (1g) were firstly crushed into powder (grain size: 180-250 µm; 80-60 mesh size), oven-dried 48 hours at 105°C and outgassed at 65°C for 4 hours under vacuum (1 µm Hg) in the apparatus. Adsorption and desorption isotherms were obtained at 77K. The relative pressure ($p/p_o$) ranges from 0.001 to 0.993 and an equilibration time of 10 s was applied during the analysis. Total pore volumes ($V_{tot}$) were determined after the liquid molar volume adsorbed at $p/p_o = 0.993$. To compare the results of two common models, the PSD was determined using both the Barrett, Johner and Halenda (BJH) and the density functional theory (DFT) methods. The isotherms were treated with the DFT model using a slit-pores model based on a 'generic surface', which is an average of non-carbon materials listed for this type of geometry. The associated potential is an averaged potential of different non-carbon materials. This model was chosen by comparing the correspondence between the

Journal Pre-proof

Cylindrical model (using an Oxide surface or the Tarazona model) and the slit-pores model. The second model was selected due to a better match with the isotherms and the lowest RMS error. The regularization rate (Smooth or Lambda) was determined individually by the intersection of the 2 curves of "RMS error of fit" and "Roughness of distribution" for each sample but was of the order of 0.3 to 1 for each. An adjustment rate R of 0.01 was applied in order to eliminate the data out-of-model (zero point of the distribution). To avoid the tensile strength effect phenomenon that occurs during desorption, the $PSD_{BJH}$ were determined from the adsorption isotherm (Barrett et al., 1951) between $p/p_0$ = 0.042 and 0.993. The Specific surface areas were calculated using the Brunauer, Emmett and Teller method (BET) for adsorption (Brunauer et al., 1938) between $p/p_0$ = 0.011 and 0.20. The external and micropore specific surface areas and pore volumes were determined using the Dubinin-Radushkevich model (DR) between $p/p_o$ ranging from 0.0001 and 0.01.

## 2. Results

### 2.1. Evolution of OM geochemical composition

After 104 days of thermal maturation at 282 to 390°C, the HI and the OI values follow the same evolution trend as those observed after 72 hours of maturation at 325°C to 470°C (Fig. 3). After maturation at 283°C, the mean calculated vitrinite reflectance (Rc) reached 0.69% ±0.07, indicating that the early oil generation stage had been reached (Tab. 1). All Rc values were confirmed by punctual vitrinite reflectance measurements taken at different stages of maturity. Hence, after thermal maturation, the measured vitrinite reflectance (Ro) is 0.71 % ±0.04. At this stage of maturity SAT+ARO hydrocarbon contents are relatively high (> 80 mg/g of TOC, > 45% of EOM) with only low concentrations of $C_1$-$C_5$ and $CO_2$ (Tab. 1, Figs. 4, 5). The amount of SAT and ARO hydrocarbons increased from M2 to E40, as a function of their hydrogen index (HI, Tab.1, Fig. 5).

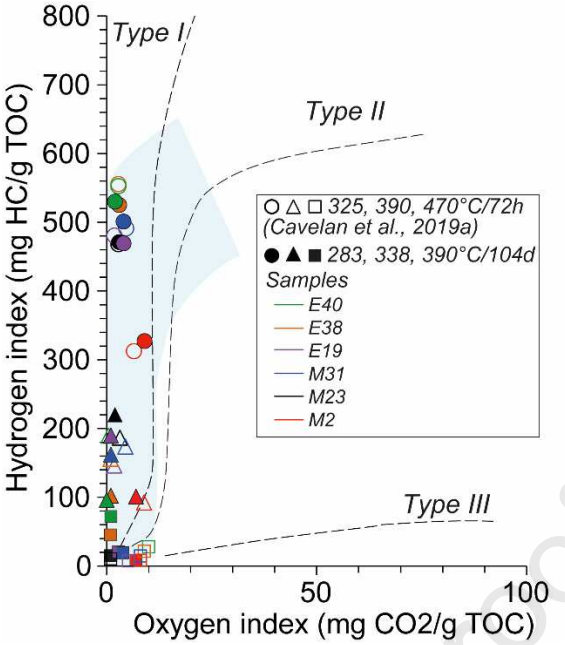



Fig. 3. Pseudo-Van Krevelen diagram showing the evolution of the hydrogen index and the oxygen index after 104 days (this study, filled symbols) and 72 hours (open symbols) of thermal maturation.

After heating at 338 and 390°C for 104 days the increase of the Rc to 1.22% ±0.10 and 2.17% ±0.12 (corresponding measured vitrinite reflectance is 1.30% ± 0.08 and 2.14% ± 0.05, respectively) indicates that the gas generation stages were reached (Tab. 1). These two stages are accompanied by a progressive and a strong increase in the concentration of $CO_2$ and $C_1$-$C_5$ gaseous hydrocarbons (Fig. 5). $C_2$-$C_5$ are the main gases generated after heating at 338°C, whereas $C_1$ is mainly produced after heating at 390°C for 104 days. The concentration of $C_1$-$C_5$ is greater for samples M31, E38 and E40, which have higher HI values (Fig. 5, Tab. 1). On the contrary, the concentration of $CO_2$ is higher for samples M2, M23 and E19, which have lower HI values (Fig. 5, Tab. 1).

Tab. 1. Mean calculated vitrinite reflectance (Rc), total extractible organic matter (EOM), total organic carbon (TOC), Hydrogen index (HI) and biomarker ratios of Kimmeridge clay samples after 104 days of maturation.

| Sample | T (C°) | TOC (wt. %) | HI (mgHC/g TOC) | EOM (mg/g TOC) | Mean $R_c$[1] (%) | Dev | Pr/Ph | Pr/n-$C_{17}$ | Ph/n-$C_{18}$ | 20S/(20S+R)[2] | 22S/(22S+R)[2] |
|---|---|---|---|---|---|---|---|---|---|---|---|
| M2 | | 3.0 | 327 | 150 | * | * | 1.07 | 1.02 | 0.63 | 0.29 | 0.50 |
| M23 | | 5.4 | 471 | 249 | 0.70 | 0.07 | 1.03 | 1.25 | 0.85 | 0.35 | 0.51 |
| M31 | 283 | 6.8 | 501 | 365 | 0.71 | 0.09 | 1.42 | 0.75 | 0.98 | 0.29 | 0.53 |
| E19 | | 10.0 | 469 | 201 | 0.72 | 0.10 | 1.08 | 0.82 | 0.52 | 0.27 | 0.49 |
| E38 | | 14.8 | 525 | 257 | 0.67 | 0.06 | 1.37 | 0.65 | 0.60 | 0.36 | 0.48 |
| E40 | | 15.4 | 530 | 366 | 0.66 | 0.03 | 1.53 | 0.74 | 1.02 | 0.42 | 0.51 |
| **Mean** | | | | | **0.69** | **0.07** | **1.25** | **0.87** | **0.77** | **0.33** | **0.50** |

Journal Pre-proof

| | | | | | | | | | |
|---|---|---|---|---|---|---|---|---|---|
| M2 | | 2.03 | 101 | 122 | 1.20 | 0.11 | 0.57 | 0.13 | 0.09 |
| M23 | | 2.22 | 220 | 181 | 1.27 | 0.14 | 0.68 | 0.08 | 0.08 |
| M31 | 338 | 4.05 | 162 | 172 | 1.22 | 0.09 | 0.76 | 0.09 | 0.13 |
| E19 | | 4.02 | 190 | 111 | 1.21 | 0.09 | 0.50 | 0.07 | 0.06 |
| E38 | | 13.27 | 102 | 116 | 1.24 | 0.12 | 0.59 | 0.04 | 0.07 |
| E40 | | 13.18 | 96 | 142 | 1.19 | 0.04 | 0.94 | 0.08 | 0.14 |
| **Mean** | | | | | **1.22** | **0.10** | **0.67** | **0.08** | **0.10** |
| M2 | | 2.35 | 9 | 35 | * | * | 0 | | |
| M23 | | 3.72 | 19 | 12 | * | * | 0 | | |
| M31 | 390 | 3.93 | 23 | 87 | * | * | 0 | | |
| E19 | | 8.47 | 34 | 27 | * | * | 0 | | |
| E38 | | 5.44 | 46 | 19 | 2.15 | 0.13 | 0 | | |
| E40 | | 5.02 | 72 | 76 | 2.19 | 0.10 | 0 | | |
| **Mean** | | | | | **2.17** | **0.12** | | | |

*Pr: pristane. Ph: phytane. *Unquantifiable ratios (very low concentrations). [1]see appendix 1. [2]20S and 20R are epimers at C-20 in the $C_{29}$ 5α,14α,17α; 22S is $C_{32}$ 17α21β 22S hopane and 22R is $C_{32}$ 17α21β 22R hopane.*

$C_{15}$-$C_{38}$ n-alkanes, accompanied by a few isoprenoids, methylated and alkylcycloalkanes (alkylcyclohexanes and pentanes), are predominant in samples up to their total degradation after heating at 390°C for 104 days (Fig. 5). Pr/n-$C_{17}$, Ph/n-$C_{18}$ and Pr/Ph ratios show a progressive decrease with increasing thermal maturity (Tab .1, Fig. 6A, B). Hopanes and steranes as well as triaromatic (TAS) and ring-C monoaromatic steroids (MAS) are quickly degraded during maturation and completely disappear after heating 104 days at 338°C (Fig. 5). 22S/(22S+R) 17α21β 22R hopane and 20S/(20S+R) $C_{29}$ 5α,14α,17α sterane ratios are > 0.30 after heating 104 days at 283°C corresponding to a maturity just below the peak of oil generation (Tab.1, Fig. 6C). Present in lower amounts, di-aromatic hydrocarbons dibenzothiophenes, naphthalenes and biphenyles) and heavier polyaromatic hydrocarbons (phenanthrenes, pyrenes and fluorenthenes) and their methylated derivatives are present in the ARO (Fig. 5). The relative proportion of some of them with increasing maturity has allowed the calculation of the mean Rc (Tab. 1, appendix 1). The n-alkanes and the di-aromatic hydrocarbon concentrations are higher for samples with the higher OM oil generation potential (M31, E40 and E38) while the concentrations of the heavier polyaromatic components are higher for the less oil-prone samples (M2, M23 and E19, Fig. 5).

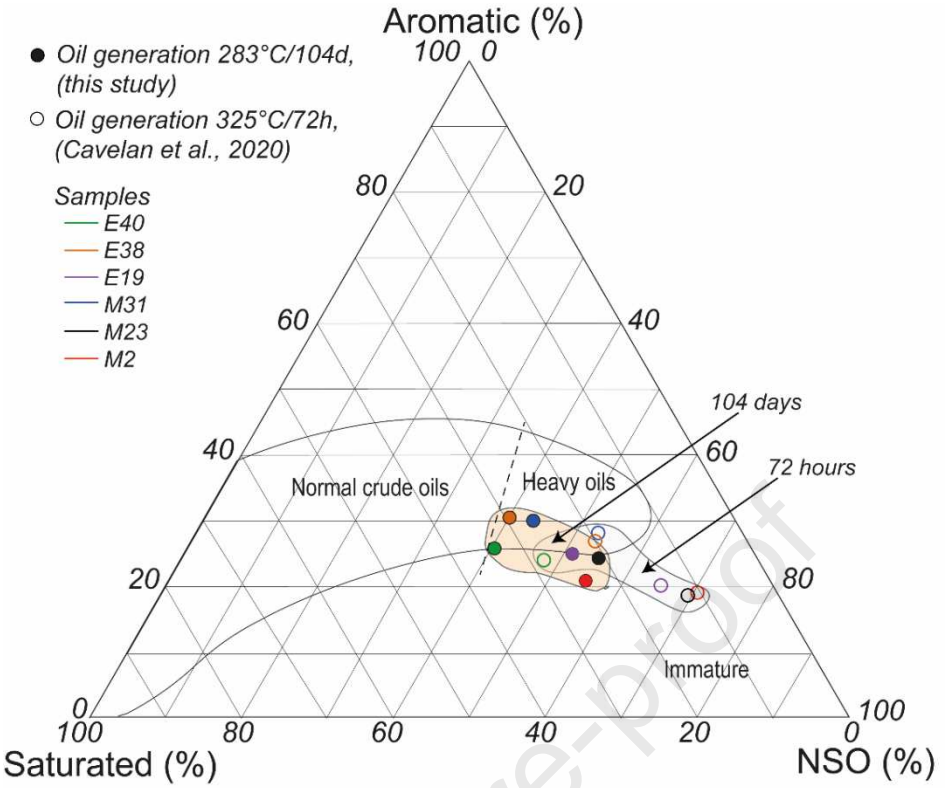



Fig. 4. Comparison of the relative proportion of saturated, aromatic hydrocarbons and NSO during oil generation (Rc of ca. 0.70%) after 104 days (filled symbols) and 72 hours (open symbols) of thermal maturation. Data of normal crude-oil from Tissot and Welte, (1984).

### 1.1. Comparison with shorter duration experiments

Comparable Rock Eval® parameters and mean Rc are obtained after maturation for 104 days and 72 hours (Fig. 3, 7A), indicating that similar stages of thermal maturity have been reached. The Rc obtained after maturation at 470°C for 72 hours (ca. 2.50%) is slightly higher than the mean Rc of 2.17% reached after maturation at 390°C for 104 days (Fig. 6A). However, the uncertainty of Rc values at this stage of maturity is greater because the concentrations of the aromatic components which served for its calculation are lower. This difference may be related only to this uncertainty attached to the calculation of the Rc. Note that the measured vitrinite reflectance values are similar between the two series: 2.12% ± 0.10 for the short-duration experiments and 2.14% ±0.05 for the long-duration experiments. Similar biomarker ratios, including 20S/(20S+R), 22S/(22S+R), pristane/phytane (Pr/Ph), Pr/n-$C_{17}$ and Ph/n-$C_{18}$ ratios are obtained after maturation for 104 days and 72 hours (Fig. 6A-C).

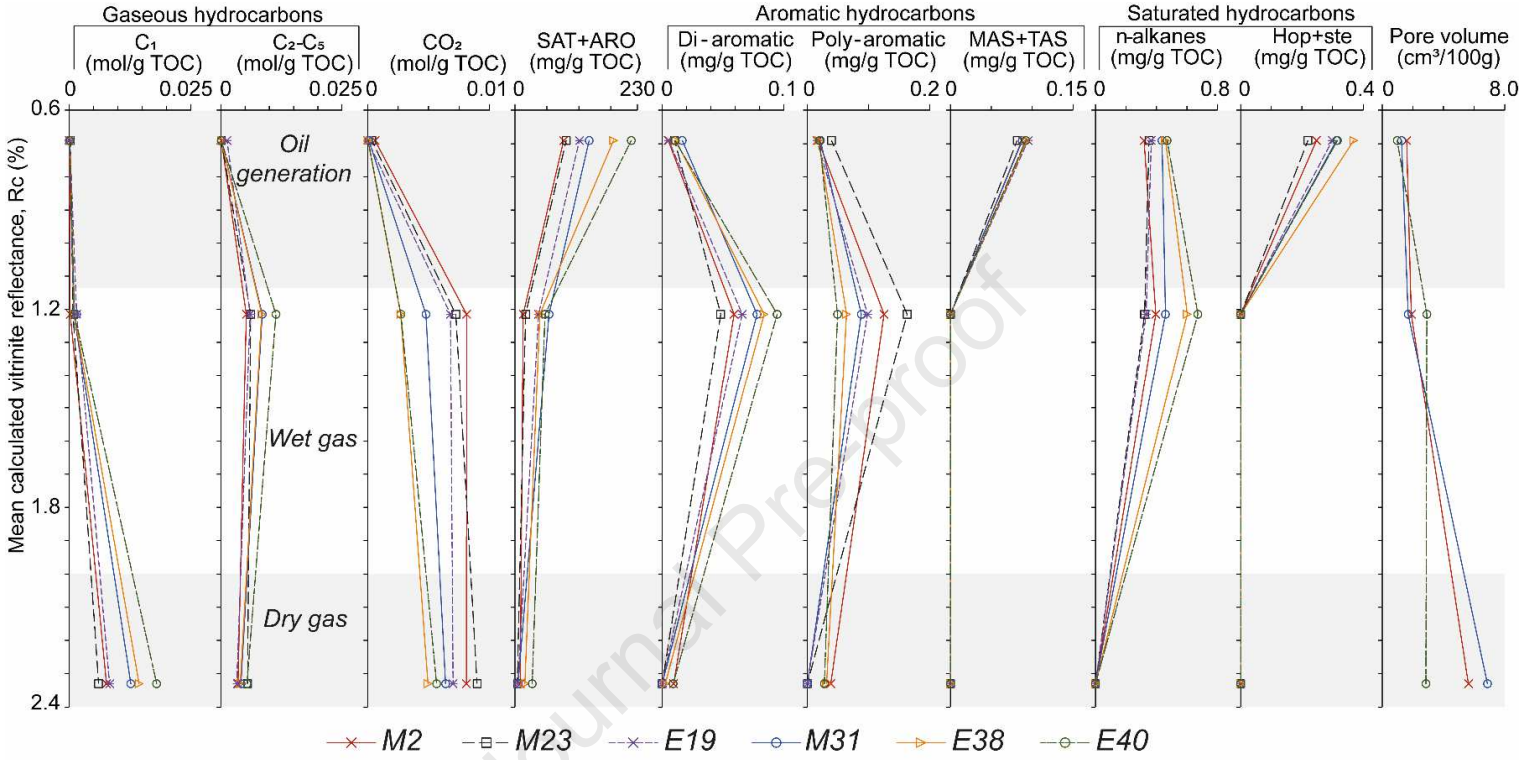



Fig. 5. Evolution of the concentrations of gas, aromatic (ARO), saturated (SAT) hydrocarbons, n-alkanes (including alkylcycloalkanes and isoalkanes), hopanes (Hop), sterane (ste), monoaromatic (MAS), triaromatic steroids (TAS), di-aromatic (dibenzothiophenes, naphthalenes, biphenyles) and poly-aromatic hydrocarbons (phenanthrenes, pyrenes, fluorenthenes) after 104 days of maturation at 283°C, 338°C and 390°C. The division of hydrocarbons generation stages (in black) is based on Rc values, Rock Eval parameters, biomarker ratios and corresponding data from the literature (Fig. 2, Landais et al., 1994).

Journal Pre-proof

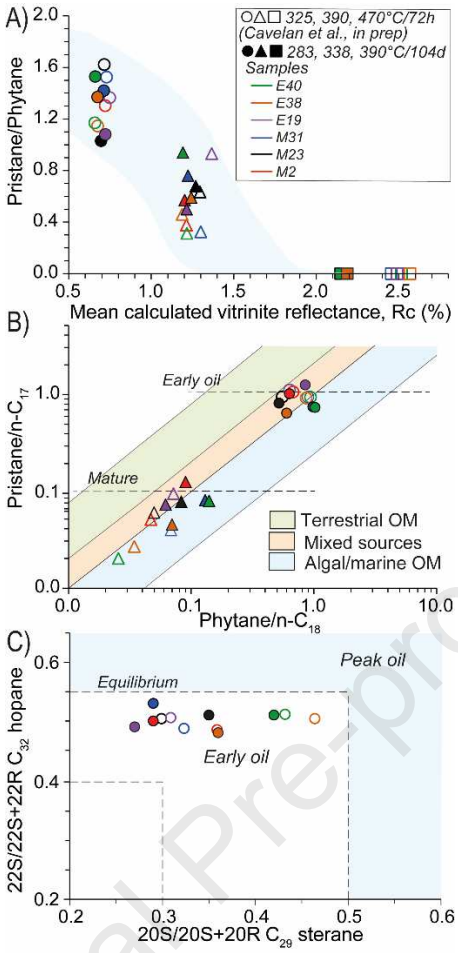



Fig. 6. Evolution of A) pristane/phytane as a function of the mean calculated vitrinite reflectance, B) pristane/n-$C_{17}$ versus phytane/n-C18, C) 22S/(22S+22R) 17α21β $C_{32}$ hopane versus 20S/(20S+20R) 5α,14α,17α $C_{29}$ sterane after 104 days (in red) and 72 hours of thermal maturation (black).

In accordance with the Rc values, the similarity of the biomarker ratios between the two series of laboratory thermal maturations suggests that similar stages of maturity have been reached after the long and the short-duration experiments. The 20S/(20S+R) value of ca.0.33 and 22S/(22S+R) value of ca.0.50 obtained after thermal maturation at 283°C for 104 days are typical values of the early oil generation stage (Fig. 6C) (Mackenzie et al., 1980; Peters et al., 2007; Seifert and Moldowan, 1981). Whatever the duration of the maturation, samples M31, E40 and E38, with the higher oil generation potential (HI> 500 mgHC/g of TOC, Tab. 1), still contain slightly lower Pr/ n-$C_{17}$ ratios for relatively high Ph/n-$C_{18}$ ratios. This indicates the presence of a less oxygenated OM (Tab. 1, Fig. 6B). As for the shorter experiments (Cavelan et al., 2019a), samples M31, E38 and E40 (higher HI values) generated higher amounts of SAT+ARO hydrocarbons enriched in alkanes, di-aromatic hydrocarbons and $C_1$-$C_5$

gaseous hydrocarbons, while M2, M23 and E19 (lower HI values) generated the highest amount of $CO_2$, lower contents of SAT+ARO richer in heavier polyaromatic components (Fig. 5). However, some differences are observable between the longer and the shorter maturation experiments. While the total concentrations of EOM generated in the early oil generation stage are similar between the two maturation series, samples matured for 104 days exhibit lower NSO, $CO_2$, $C_1$-$C_5$ and slightly higher SAT, ARO, and alkane concentrations (including n-alkanes but also branched alkanes, methylalkanes, isoprenoids and alkylcycloalkanes) than samples matured for 72 hours (Figs. 4, 7). The relative proportions of SAT, ARO and NSO after 104 days of maturation are closer to the composition of the natural crude oils from Tissot and Welte, (1984) (Fig. 4). The difference in alkane concentrations is more pronounced for samples with the higher OM oil generation potential (IH >500 mgHC/g TOC): M31, E38 and E40 (Fig. 7). Similar concentrations of poly- and di-aromatic hydrocarbons are obtained.

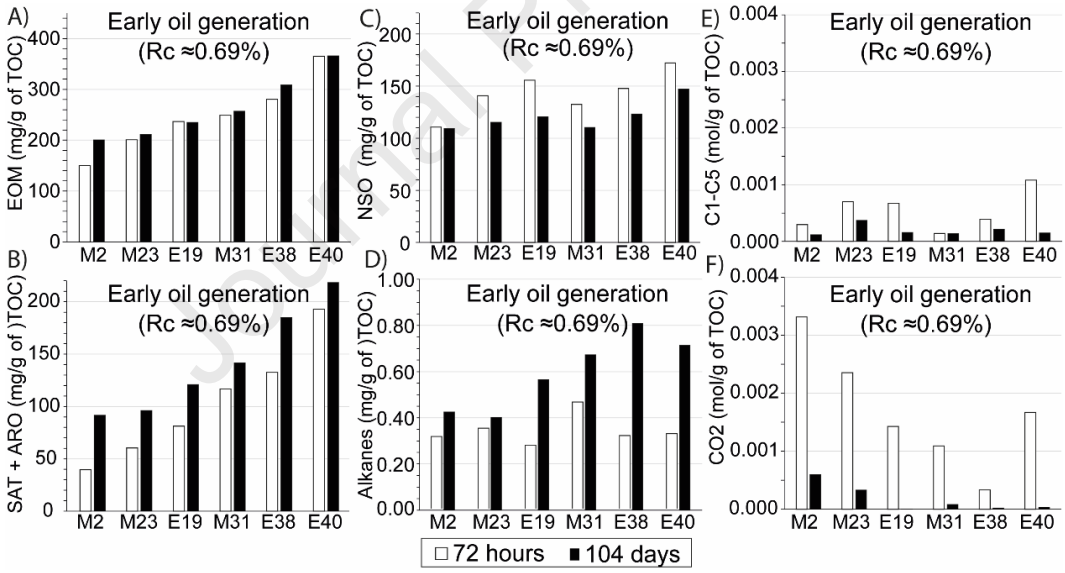



Fig. 7. Comparison of A) extractible organic matter (EOM), B) saturated (SAT), aromatic (ARO) hydrocarbons, C) NSO, D) alkanes (hopanes, steranes, n-alkanes, branched alkanes, isoprenoids and alkylcycloalkanes), E) $C_1$-$C_5$ gaseous hydrocarbons and F) $CO_2$ concentrations in the early oil generation stage after 104 days and 72 hours of thermal maturation. The division of hydrocarbons generation stages is based on Rc values, Rock Eval parameters, biomarker ratios and Fig.2.

Journal Pre-proof

In the condensate wet gas zone, the increase in the maturation duration resulted in the production of higher $C_2$-$C_5$ concentrations for samples with the higher oil generation potential (M31-E40), lower $C_1$ and lower $CO_2$ concentrations (Fig. 8). Comparable alkane and di-aromatic hydrocarbon concentrations are obtained in the condensate wet gas zone after maturation for 104 days and 72 hours. However, significantly lower concentrations of poly-aromatic hydrocarbons are observed after maturation for 104 days (Fig. 8E). The concentration of polyaromatic hydrocarbons decreases from the sample M2 and E40 as a function of the initial oil generation potential of the samples (Fig.8E). Lower NSO concentrations are obtained for most of the samples from the longer duration experiment (Fig. 8C).

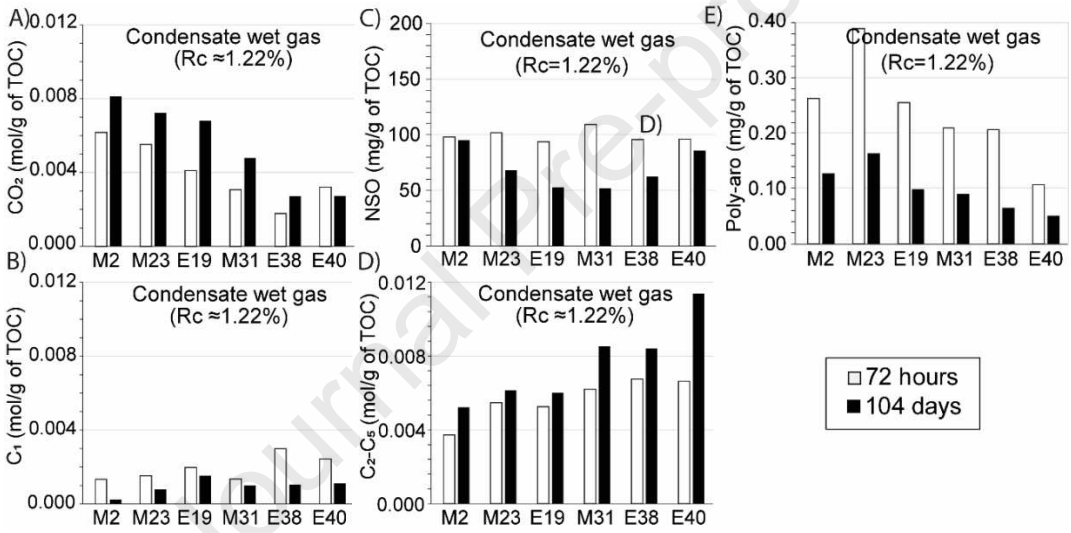



Fig.8. Comparison of the concentrations of A) $CO_2$, B) $C_1$, C) NSO, D) $C_2$-$C_5$ gases and E) selected polyaromatic hydrocarbons (phenanthrenes, pyrenes and fluorenthenes) in the condensate wet gas zone after 104 days and 72 hours of thermal maturation. The division of hydrocarbons generation stages is based on Rc values, Rock Eval parameters, biomarker ratios and Fig.2.

Journal Pre-proof

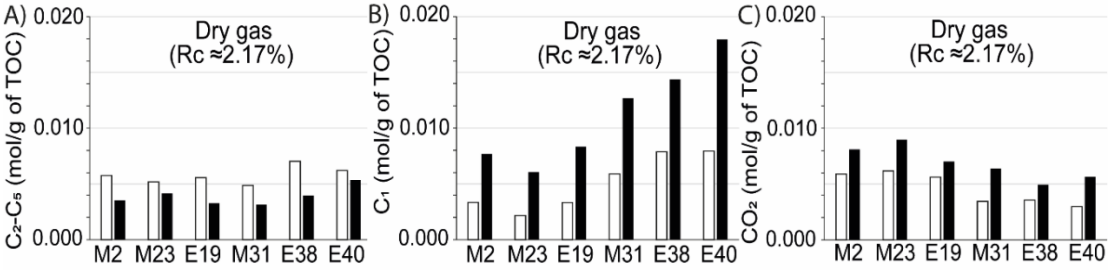



Fig. 9. Comparison of A) $C_2$-$C_5$, B) $C_1$ and C) $CO_2$ concentrations in the dry gas zone after 72 hours (Cavelan et al., 2019a) and 104 days (this study) of thermal maturation. The hydrogen index increases from samples B2 to E40. The division of hydrocarbons generation stages is based on Rc, Rock Eval parameters, biomarker ratios and corresponding data from the literature.

In the dry gas zone, the increase in the duration of maturation allows the production of higher $C_1$ concentrations and still higher concentrations of $CO_2$ (Fig. 9). $C_2$-$C_5$ are, however, present in slightly lower amounts after maturation for 104 days in the dry gas zone (Fig. 9A). The concentration of residual NSO, poly- and di-aromatic hydrocarbons are too low at this stage of maturity to allow a good comparison between the two series. The concentration of $C_1$ increases from M31 to E40 as a function of the initial oil generation potential of the OM (Fig.9B) while the concentration of $CO_2$ decreases (Fig.9C).

### 1.2. Evolution of pore volume and surface area after 104 days of maturation

#### 1.2.1.Isotherms

An example of the evolution of nitrogen adsorption and desorption isotherms at 77K with increasing maturity is presented in Fig. 10. Whatever their initial composition and maturity, all samples show type IV isotherms, indicating the presence of mainly mesoporous materials (Sing, 1985). The shape of the hysteresis loops indicates the presence of pores with slit-shaped associated with aggregated plate-like particles (Sing, 1985). However, in natural materials such as shale rocks, previous studies (Clarkson et al., 2013; Schmitt et al., 2013) revealed that the assumption of slit-shaped pores could be subjected to error, and thus has to be considered with caution.

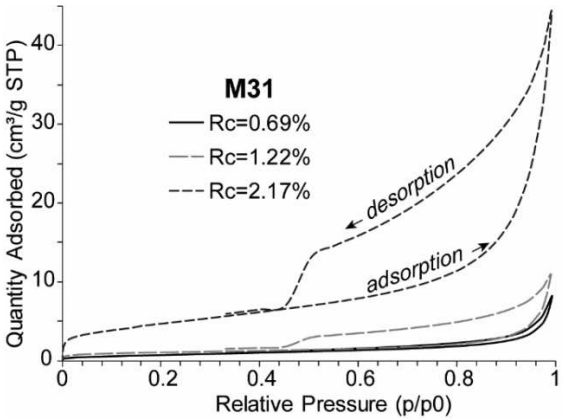



Fig. 101. Example of the evolution of KCF samples' nitrogen gas adsorption and desorption isotherms (at 77K) with increasing thermal maturity.

The volume of gas adsorbed around $p/p_0$ = 0.992 is low after maturation at 283°C for 104 days (Rc=0.69%, Fig. 10). After maturation at 338°C and 390°C for 104 days, the volume of gas adsorbed increases progressively, indicating the increase in sample pore volumes.

### 1.2.2.Pore volumes, specific surface areas and pore size

The total pore volumes (Vp) and the BET specific surface areas ($S_{BET}$) of samples are low after heating at 283°C for 104 days (Tab. 2). At this maturation stage, the Vp (≤1.59 cm3/100g) and the $S_{BET}$ (≤ 9.31 $m^2/g$) decrease from M2 to E40, and thus decrease with the increase in the initial OM oil generation potential. The PSD determined using the DFT and the BJH methods give similar results (Figs. 11, 12) and show that all KCF samples exhibit a large pore size distribution mainly ranging from meso to macropores (Fig. 12) after maturation at 283°C for 104 days. The BJH method was used to characterize the mesoporosity, the DFT was used to determine the mesoporosity and part of the microporosity, and the DR was used to assess the microporosity. A comparison of the surface areas and the pore volume calculated with these different models with the $S_{BET}$ and the Vp enabled the relative contribution of the meso and the micropore surface area and pore volume of each sample to be estimated.

Tab. 2. Total pore volumes ($V_p$), BET specific surface areas ($S_{BET}$), surface areas ($S_{BJH}$) and pore volumes ($V_{BJH}$) determined using the Barrett, Johner and Halenda method (BJH) (adsorption

Journal Pre-proof

isotherms) and the density functional theory (DFT), micropore volumes ($V_{micro}$) and micropore surface areas ($S_{micro}$) determined using the Dubinin-Radushkevich models (DR) for three representative samples after 104 days of thermal maturation.

| Sample | T (°C) | $V_p$ (cm3/100g) | $S_{BET}$ ($m^2/g$) | $S_{BJH}$ ($m^2/g$) | $V_{BJH}$ (cm3/100g) | $S_{BJH}$ / $S_{BET}$ | $S_{DFT}$ ($m^2/g$) | $V_{DFT}$ (cm3/100g) | $S_{DFT}$ / $S_{BET}$ | $S_{micro, DR}$ ($m^2/g$) | $V_{micro, DR}$ (cm3/100g) | $S_{DR}$/ $S_{BET}$ | $V_{DR}$/ Vt (%) |
|---|---|---|---|---|---|---|---|---|---|---|---|---|---|
| M2 | | 1.59 | 9.31 | 3.1 | 1.2 | 0.35 | 5.92 | 1.49 | 0.64 | 9.99 | 0.35 | 1.13 | 22.3 |
| M31 | 283 | 1.26 | 2.64 | 1.7 | 1.19 | 0.64 | 1.55 | 1.12 | 0.59 | 2.02 | 0.07 | 0.77 | 5.7 |
| E40 | | 0.97 | 1.89 | 1.24 | 0.92 | 0.69 | 1.05 | 0.95 | 0.55 | 1.18 | 0.04 | 0.65 | 4.3 |
| M2 | | 1.89 | 3.76 | 2.63 | 1.82 | 0.7 | 2.46 | 1.76 | 0.65 | 4.18 | 0.15 | 1.11 | 7.9 |
| M31 | 338 | 1.69 | 3.6 | 2.04 | 1.62 | 0.57 | 2.23 | 1.55 | 0.62 | 4.02 | 0.14 | 1.12 | 8.5 |
| E40 | | 2.91 | 6.61 | 3.33 | 2.72 | 0.5 | 3.9 | 2.74 | 0.59 | 5.57 | 0.2 | 0.84 | 6.8 |
| M2 | | 5.62 | 19.5 | 18.22 | 5.08 | 0.94 | 14.36 | 5.25 | 0.74 | 20.92 | 0.74 | 1.33 | 13.2 |
| M31 | 390 | 6.87 | 16.9 | 11.21 | 6.49 | 0.67 | 11.36 | 6.47 | 0.67 | 16.56 | 0.59 | 0.97 | 8.6 |
| E40 | | 2.85 | 5.36 | 3.83 | 2.75 | 0.72 | 3.04 | 2.81 | 0.57 | 3.97 | 0.14 | 0.74 | 4.9 |

As shown by the pore volume determined using the BJH ($V_{BJH}$) close to the $V_p$, most of the pore volume is provided by meso and macropores in the studied samples (Tab. 2). However, contrary to the other two samples, the lower $S_{BJH}$/ $S_{BET}$ ratio, far from 1.0, the slightly higher $S_{DFT}$ / $S_{BET}$ ratio and especially the higher $S_{DR}$ / $S_{BET}$ ratio close to 1 after heating at 283°C indicate that most of the specific surface area of the sample M2 is provided by micropores (Tab. 2). The $V_{DR}$/Vt ratio indicates that micropores account for about 22% of the total pore volume in this sample and less than 6% in the other two samples. This is well substantiated by the PSD from the DFT methods, which showed the presence of two controlled-size porosities about 1.3 and 4 nm in diameter in M2 (Fig. 12). These porosities have a significant contribution to the total specific surface area after maturation at 283°C for 104 days.

Journal Pre-proof

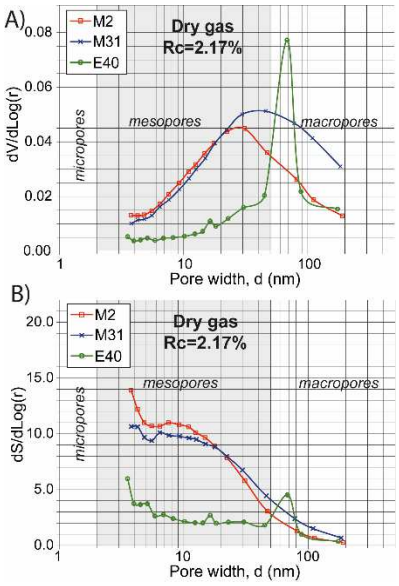



Fig. 11. BJH A) pore size and B) surface area distributions of samples M2, M31 and E40 after thermal maturation at 390°C for 104 days.

After heating at 338°C for 104 days, the $V_p$, the $V_{BJH,\ ads}$ and the $V_{DFT}$ increase (Tab. 2, Fig. 5). While the $S_{BET}$ increases for M31 and E40, $S_{BET}$ strongly decreases for M2 due to the decrease in its number of micropores around 1.3 nm in diameter after maturation at 338°C (Tab. 2, Fig. 12). E40, the highly oil-prone sample, exhibits higher $V_p$ and $S_{BET}$ than M2 and M31, which show similar features (Tab. 2). The differences between samples are less significant at this thermal maturity. All samples exhibit a similar PSD, with a predominance of mesopores ranging mainly from 4 to 150 nm in diameter (Fig. 12).

As shown by the $V_{BJH}$ close to the $V_p$, these mesopores account for most of the pore volume after maturation at 338°C. The PSD from the DFT, however, shows the presence of a controlled size microporosity around 1.3 nm with a relatively low contribution to the pore volume ($V_{DR}$/Vt of ca. 8%, Tab. 2, Fig. 12) but a significant contribution to the specific surface area. This feature may explain the $S_{DR}$ / $S_{BET}$ ratio close to 1 in all samples and the $S_{DFT}$ / $S_{BET}$ and $S_{BJH}$ / $S_{BET}$ ratios far from 1.0 (Tab. 2). As shown by the $V_{DR}/V_t$ (%), these micropores account for about 8% of the pore volume of KCF samples after maturation at 338°C for 104 days. After maturation at 390°C for 104 days, the $V_p$ and the $S_{BET}$ increase strongly except for E40 for which these values remain relatively stable (Tab. 2, Fig. 5).

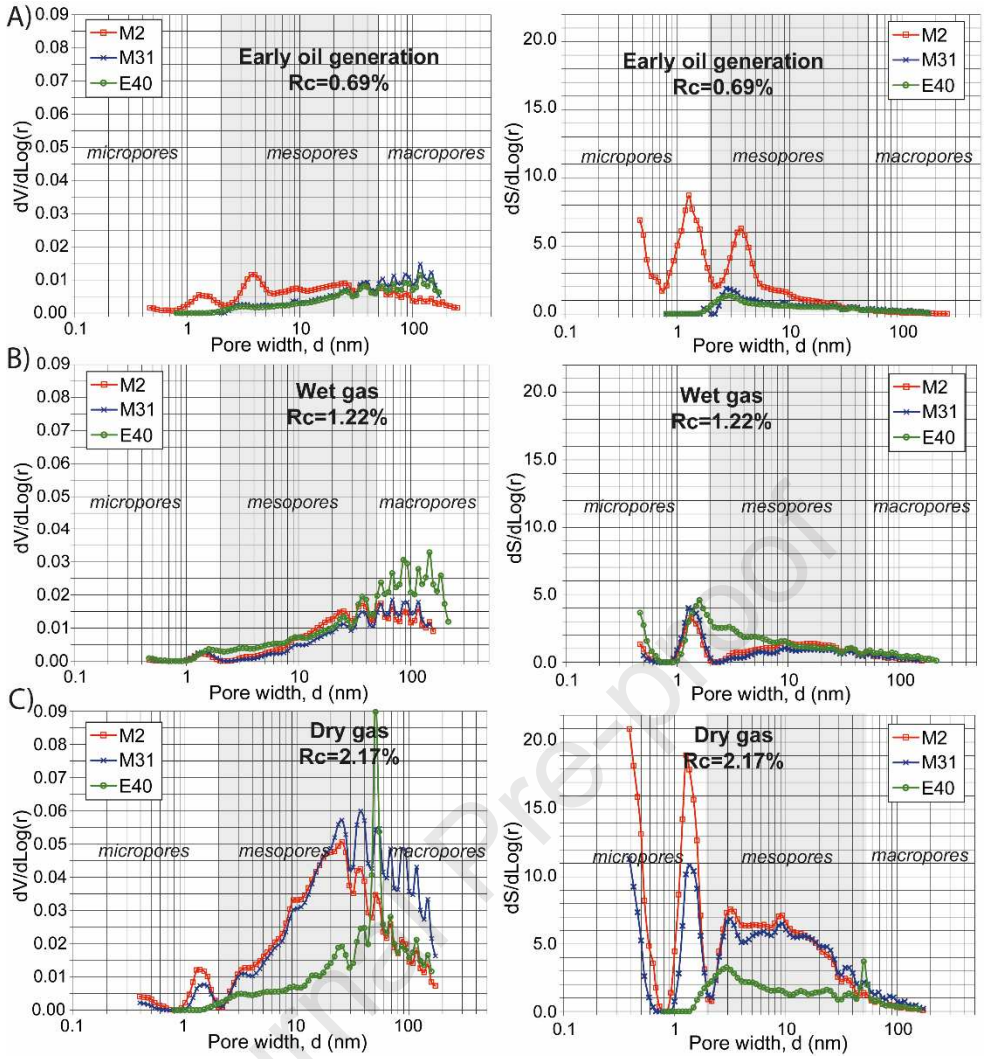



Fig. 12. DFT pore size (left) and surface area distribution (right) of samples M2, M31 and E40 after thermal maturation at A) 283°C, B) 338°C and C) 390°C for 104 days.

The Vp and the $S_{BET}$ thus decrease with the increase in the initial TOC and OM oil generation potential. The $V_{BJH}$ still close to the $V_p$ indicate that the total pore volume of samples is still mainly provided by meso and macropores (Tab. 2), widely distributed between 2 and 150 nm after maturation at 390°C for 104 days (Figs. 11, 12). The PSD from the DFT, however, shows the increase in the number of pores at ≈1.3 nm and 4 nm for M2 and M31 (Fig. 12). While these micro and small mesopores make a relatively low contribution to the total pore volume ($V_{DR}/V_t$ ratio between 8.6% and 13.2%), they provide a significant part of the specific surface area marked by a high DR micropore surface area ($S_{DR}$) (Fig. 12, Tab. 2). The PSD from the DFT method suggest that micropores less than

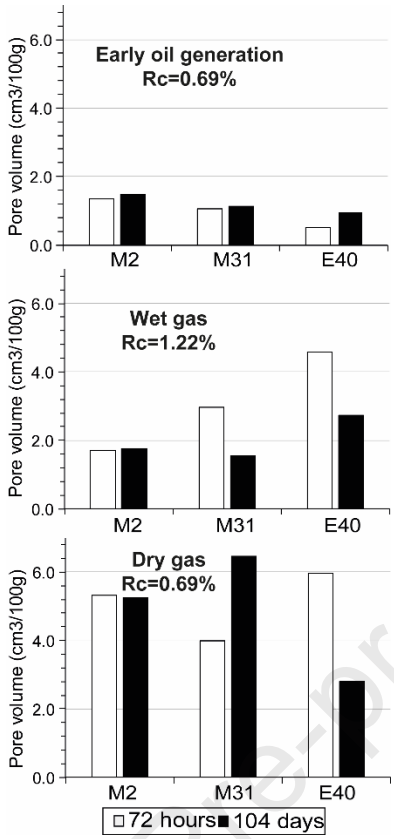
Journal Pre-proof

0.4 nm in diameter with a high contribution to the specific surface area are present after heating at 390°C for 104 days but are not quantifiable by nitrogen adsorption.

#### 1.2.3. Comparison of porosity evolution with shorter duration experiments.

Similar trends in pore volume evolution are observed after 104 days (Fig. 5, this study) and 72 hours (Cavelan et al., 2019a) of thermal maturation. The total pore volume, very low in the early oil generation stage, increases progressively to the dry gas zone (Fig. 5). While no real differences are observed during oil generation, some slight differences are, however, visible between the two series during gas generation (Fig. 13). Slightly lower pore volumes are observed in the condensate wet gas zone. Increasing the duration of thermal maturation does not allow the formation of a greater pore volume at this stage of maturity. In the dry gas zone, the relation between the pore volume and the thermal maturation duration is not clear. While M2 exhibits a similar pore volume after maturation for 72 hours and 104 days, M31 exhibits a higher pore volume and E40 a lower pore volume after maturation for 104 days (Fig. 13). Despite the fact that all samples exhibit a similar porosity mainly composed of widely distributed mesopores and macropores, differences in PSD are observed after 104 days (Fig. 12) and 72 hours of thermal maturation (Cavelan et al., 2019a), especially in the condensate wet gas zone. Contrary to the results from Cavelan et al. (2019a), where highly oil prone samples contain mainly pores < 10 nm and less oil prone samples contain pores > 10 nm, less important differences of PSD are observed between our samples after 104 days of maturation (Fig. 12). The pores are mainly comprised between 1 and 80 nm in diameter.

Journal Pre-proof




156

157 Fig. 13. Comparison of total pore volumes after 104 days (this study) and 72 hours (Cavelan et al.,
158 2019a) of thermal maturation at different maturities.

159 **2. Discussion**

160 **2.1. How useful is it to combine different models for nitrogen adsorption measurements?**

161 The concomitant use of different models for nitrogen adsorption measurements, such as the DFT and
162 the DR, enables to learn more about the pore structure of KCF rocks. In accordance with BJH pore
163 size distribution and previous work, DFT pore size distributions show that most of the remaining pore
164 volume in KCF rocks is provided by meso and macropores which vary widely in diameter from 2 to
165 160 nm in the early oil generation stage. However, the PSD curves from the DFT, which are more
166 precise for microporosity and small mesoporosity assessment, reveal the presence of two controlled-
167 size porosities at about 1.3 and 4 nm in diameter, only visible in the sample with the lowest oil
168 generation potential in the early oil generation stage (M2, Fig. 12). These two controlled-size
169 porosities are also observed in the condensate wet gas zone and are clearly visible in M2 and M31 in
170 the dry gas zone (Fig. 12). According to the shape of the isotherms hysteresis loops (Fig. 10), these

Journal Pre-proof

171 micro and small regular mesoporosity could correspond to slit-shaped pores associated with the plate-
172 like clay particle aggregates previously observed in KCF rocks using SEM imaging (Cavelan et al.,
173 2019b). While these small meso and micropores generally make a limited contribution to the pore
174 volume, they provide a high specific surface area (Fig. 12) at the origin of the higher total BET and
175 DR specific surface area of M2. Their role in gas storage and adsorption phenomena should thus not
176 be neglected. In previous SEM images, the phytoplanktonic orange AOM, abundant in oil-prone
177 rocks, appeared as a 'gel' which seems to fill the interlayer space between minerals, reducing the
178 mineral associated pore volume of certain samples before maturation (Cavelan et al., 2019b). We can
179 thus suggest that M31 and E40, which initially contain significantly higher amounts of orange AOM
180 than M2 (Cavelan et al., 2019a), exhibit initially a lower micro and mesoporosity associated with clay
181 sheet aggregates. Then, the filling of the porosity of these two higher oil prone samples by effluents
182 during oil generation makes the rest of these pores inaccessible to nitrogen adsorption. Hence their
183 lower porosity at 1.3 and 4 nm in diameter during oil generation (Fig. 12). During the progressive
184 conversion of residual OM and oil into gaseous hydrocarbons and the ensuing generation of secondary
185 pores in OM, some micro and mesopores associated with clay minerals may be progressively released
186 and/or become more accessible to nitrogen adsorption. This probably explains their increasing
187 contribution to the pore volume and the specific surface area (increase in $S_{micro,\ DR}$ and $V_{micro,\ DR,}$) from
188 the condensate wet gas to the dry gas zone in samples M2 and M31 (Tab. 2, Fig. 12). Indeed, the $S_{DR}$ /
189 $S_{BET} \geq 1$ in M2 and M31 indicates that most of the specific surface area is provided by micropores
190 (Tab. 2). In the sample E40, a more extensive collapses/alteration of the pore structure in response to
191 its important gas generation may have limited the accessibility of these pores to nitrogen adsorption,
192 explaining the absence of pores 1.3 nm in diameter in the dry gas zone (Fig. 12). Although this
193 relatively scarce porosity associated with clay sheet aggregates makes a small contribution to the total
194 pore volume, it is a major contributor to the specific surface area and may have a significant ability to
195 adsorb and retain gas. These pores could thus also contribute to the gas storage capacity of these
196 source rocks.

197 **2.2. Effect of the duration of confined thermal maturation on OM thermal degradation**

Journal Pre-proof

As previously demonstrated (Landais et al., 1994; Wood, 1988), different time-temperature pairs can thus be used to reach the same stage of maturity. As expected, comparable Rc and thermal maturity biomarker ratios are obtained after thermal maturation for 72 hours (Cavelan et al., 2020) and 104 days, indicating indeed that similar stages of maturity have been reached: the early oil generation (Rc ca. 0.70%), the condensate/wet gas (Rc ca. 1.23%) and the dry gas zone (Rc: 2.2-2.5%) (Tab. 1, Fig. 6). It is thus possible to compare the bulk, the molecular composition of OM and the porosity between the two series as a function of the duration of maturation experiments. Our results show that Pr/Ph, Pr/n-$C_{17}$, Ph/n-$C_{18}$ ratios and the relative proportion of the different hopane and sterane configurations do not depend on the duration of the maturation (Tab. 1, Fig. 6). The Rock Eval® parameters do not exhibit variations related to the duration-temperature pairs chosen for the experiments (Fig. 3). This well substantiates the results of Landais et al. (1994) on type II source rocks and OM isolated from the Paris basin. Similar evolution of EOM, $CO_2$ and $C_1$-$C_5$ concentrations and comparable OM components with similar distributions are observed in SAT and ARO fractions for long (104 days) (Fig. 5) and short (72 hours) maturation experiments. Furthermore, the choice of the time-temperature pairs does not influence the differences observed between samples with various initial oil generation potential. In both cases, the concentration of EOM (especially of SAT and ARO), alkanes and di-aromatic hydrocarbons in the early oil generation stage and thus the concentration of $C_1$-$C_5$ hydrocarbon gases during gas generation increase with the OM oil generation potential (Fig. 5). These longer maturation experiments thus confirm the influence of the slight variations in the initial OM composition of KCF mudstones on the amount and the composition of EOM generated, as previously discussed (Cavelan et al., 2020, 2019a).

However, some differences are visible between the two series during oil and gas production. Shorter duration experiments (72 hours) appear to favor the production of EOM enriched in NSO, while long-duration experiments (104 days) seem to favor the production of EOM enriched in SAT and, to a lesser extent, ARO hydrocarbons in the early oil generation stage (Figs. 4, 7). The relative proportion in EOM of SAT and ARO hydrocarbons appears thus closer to the composition of natural crude oils (Fig. 4). Hence, residual EOM exhibit lower NSO and especially lower polyaromatic

Journal Pre-proof

concentrations such as phenanthrenes, pyrenes or fluorenthenes during gas generation stages (Fig. 8). The increase in the maturation duration, and thus the increase in the residence time in the thermal maturation system, appears to enhance the degradation of heavy NSO components into SAT and ARO hydrocarbons. This probably explains the higher alkane concentrations in the SAT fraction after the long-duration experiment in the early oil generation stage (Fig. 7). Similar results were previously found on type II Paris Basin source rocks and type III Mahakam coal (Landais, 1991; Landais et al., 1994). On the contrary, lower $C_1$-$C_5$ concentrations are generated in the early oil generation stage after the long- duration experiment (Fig. 7). As previously suggested by Landais et al. (1994), the lower temperature used for the long-duration experiment (283°C for 104 days) probably led to a less pronounced early cracking of OM into light components by preventing low energy bonds from being broken during the early stage of maturation. This may also explain the slightly lower $C_1$ concentration for the longer duration experiment in the condensate/wet gas (Fig. 8). This lower early transformation of OM then leads to a more efficient secondary cracking of OM at higher maturity stages. This results in higher $C_2$-$C_5$ concentrations in the condensate wet gas zone and to a more efficient conversion of $C_2$-$C_5$ into $C_1$ in the dry gas zone responsible for the lower remaining $C_2$-$C_5$ concentrations and the significantly higher $C_1$ concentration of the longer maturation experiment (Figs. 8, 9). Note, however, that contrary to the Paris basin source rocks, where $CO_2$ concentrations did not appear to be influenced by these processes (Landais et al., 1994), increasing the duration of the experiments in the KCF also seems to lead to the production of lower $CO_2$ concentrations in the early oil generation stage but higher concentrations during gas generation (Figs. 7-9). Nevertheless, the difference in $CO_2$ concentrations between the two series seems to depend on the initial OM composition of KCF samples, especially during condensate wet gas generation. This difference, which is significant for the less oil-prone samples (M2 to E19), does not exist in the two highly oil-prone samples (E38 and E40, Fig. 8). This suggests that the effect of the duration-temperature pair choice on OM thermal degradation may also slightly depend on the original OM composition and oil generation potential.

After the long-duration experiments, the concentrations of $C_2$-$C_5$ are still very high in the dry gas zone compared to the concentrations of $C_1$ (Fig.5). All biomarker ratios and Rc values (verified by

Journal Pre-proof

punctual vitrinite reflectance measurements) indicate that the dry gas zone has been reached after maturation at 390°C for 204 days. However, based on gas concentrations alone, the production and the composition of gaseous hydrocarbons are closer to those of the middle/end of the condensate/wet gas zone. These differences were also visible for short-duration experiments, but were more pronounced (Cavelan et al., 2020). The conversion of $C_2$-$C_5$ gaseous hydrocarbons into methane was delayed during the short and the long-duration experiments, leading to a discrepancy between the predicted maturity (Rc, biomarkers) and the real thermal maturity of the OM. Despite a significant increase in thermal maturation duration, the composition of the gaseous hydrocarbons generated by laboratory experiments remains somewhat different from those obtain under low temperature, after long-duration geologic maturations. Moreover, artificial thermal maturations were carried out on powdered samples and under an external hydrostatic confining pressure. This cannot accurately reproduce the effect of the lithostatic pressure that affect the structure of the rock in sedimentary basins. During laboratory thermal maturations, the pressure is transmitted into the rock by the effluents (water, hydrocarbons and gases). The relation between porosity, oil expulsion and retention processes is thus not accurately simulated. This may impact both the OM thermal degradation and the development of pores. Nevertheless, the pore volumes obtained during artificial maturations (ranging from 0.97 cm3/g to 6.87 cm3/g) are very consistent with those of naturally-matured organic-rich shales. For example, Mastalerz et al. (2013), Milliken et al. (2013), Pan et al. (2015), Song et al. (2019), among many others, found similar porosity and pore volumes in their naturally-matured samples for similar maturities. Artificial thermal maturation remains therefore a good technique to study the porosity of shales at different thermal maturities, despite the differences with regard to natural sedimentary basins.

### 2.3. Does the duration of confined thermal maturation affect the evolution of porosity?

Similar variations in pore volume are observed from the early oil generation to the dry gas zone after 104 days (this study, Fig. 5) and 72 hours of thermal maturation (Cavelan et al., 2020, 2019a). Total pore volumes and specific surface areas are very low during early oil generation (probably filled/occluded by oil) and then exhibit a progressive increase (probably due to the formation of pores in OM), which depends on the initial OM oil generation potential (Fig. 5). The more a sample has

Journal Pre-proof

produced hydrocarbons (especially light saturated compounds) able to migrate and fill the adjacent porosity, the smaller the pore volume is during oil generation. This was observed during the short-duration and the long-duration experiments. Indeed, samples with a higher OM oil-generation potential (such as E40) have lost a higher volume of pores during oil generation, occluded by the larger quantity of SAT and ARO generated (Tab. 2). The increase in maturation duration allows the production of less viscous EOM enriched in SAT and ARO hydrocarbons, but this does not influence the total amount of EOM generated during oil generation (Fig. 7). This probably explains why similar BJH pore size distributions and similar pore volumes are observed after 72 hours and 104 days of maturation in the early oil generation stage (Fig. 13). The slight differences of SAT, ARO and NSO relative proportions between the two series appear thus to have a limited effect on pore occlusion processes during the early stages of maturation. This well substantiates the hypothesis that a link exists between the OM composition, its capacity to generate hydrocarbons and the evolution of porosity.

In most of the studies carried out on organic-rich shales, gas generation coincides with the development of abundant pores in OM, in response to the production and the expulsion of gaseous hydrocarbons (Bernard et al., 2012b; Curtis et al., 2012; Han et al., 2017; Ko et al., 2018; Loucks et al., 2012; Song et al., 2019; Y. Wang et al., 2020; Wu et al., 2019, among many others). This formation of pores was also observed in the KCF after short-duration thermal maturation experiments (Cavelan et al., 2020, 2019a). However, these results showed that the massive production of gaseous hydrocarbons may lead to deformations of the OM structure that may cause the decrease of the pore volume at the end of the condensate/wet gas zone, especially for the highly oil-prone samples (such as E40) which generated higher concentrations of gaseous hydrocarbons. We can suggest that a more unstable pore network, particularly sensitive to pressure-induced deformations (tied to the presence of more abundant and well-connected gas devolatilization vacuoles), formed in the highly oil-prone rocks in response to the massive generation of gaseous hydrocarbons. The increase in maturation duration causes an increase in the amount of $C_2$-$C_5$ generated in the condensate wet gas zone, especially for samples with a higher OM oil generation potential (such as E40, Fig. 8). These samples may thus have suffered earlier or more pronounced alteration of their pore network in response to the more important

Journal Pre-proof

generation of gaseous hydrocarbons, leading to slightly lower pore volumes than for the shorter duration experiments (Fig. 13). The less oil-prone sample M2 generates relatively similar amounts of gaseous hydrocarbons after heating for 72 hours and 104 days (Figs. 8) and exhibits comparable pore volume and PSD (pores widely distributed from 8 to 160 nm in diameter) in the condensate wet gas zone. This provides support for this hypothesis (Fig. 13). A different timing and amplitude of the alteration of the pore network in response to the different amounts of gaseous hydrocarbons generated between the two series of maturation may explain the different PSD observed for the highly oil-prone samples M31 and E40. After maturation for 72 hours, M31 and E40 are composed of meso and micropores less than 40 nm (Cavelan et al., 2019a), while they contain mainly meso and macropores more than 8 nm after heating for 104 days (Fig. 12). We can suggest that the lower temperature used by the longer maturation experiments, which seems to prevent the lower energy bonds from being broken early on, may result in a slower and more homogeneous gas generation throughout the OM particles forming a better interconnected and distributed OM-hosted porosity in the condensate wet gas zone. Despite frequent collapse/alteration events, this may have enhanced early pore coalescence at the origin of the larger pore sizes after heating for 104 days.

In the dry gas zone, as previously observed after maturation for 72 hours, the specific surface area and the pore volume of samples increase more or less as a function of the initial OM composition and gas concentrations (Tab. 2). Moreover, the PSD indicates a comparable porosity mainly composed of pores larger than 10 nm in the two series. As observed during the short-duration experiments, the sample with the highest OM oil generation potential (E40) generated higher amounts of SAT and ARO enriched in hydrogenated components (such as n-alkanes) and exhibits lower pore volume than less oil prone samples in the dry gas zone (Fig. 13). This confirms that the pore volume formed during gas generation is not linearly correlated with the OM oil generation potential. However, the slightly different timing of generation and concentrations of $C_1$-$C_5$ gaseous hydrocarbon has probably influenced the ability of the rock to preserve its pore network from collapse or deformation events that have affected the pore volume, probably causing the differences in pore volume between samples of the two series of maturation. Our results show that increasing the duration of thermal maturation

Journal Pre-proof

experiments influences the composition of EOM, the amount and the timing at which gaseous hydrocarbons are generated. Nevertheless, these differences, relatively small between 72h and 104 days of maturation, do not significantly affect the development and the evolution of KCF mudstones' porosity with increasing maturity. Similar trends of pore volume and specific surface area are observed with increasing maturity and similar variations of porosity are observed between samples with a slightly different initial OM composition. The choice of duration-temperature pairs for thermal maturation experiments seems thus to have a limited impact on the porosity of organic-rich source rocks.

## Conclusions

The comparison between short-duration (72h) and long-duration thermal maturations of organic-rich mudstones shows that, for a same thermal maturity, increasing the duration of thermal maturation experiments: (i) does not influence the amount of EOM generated; (ii) increases the residence time of the effluents in the thermal maturation system, enhancing the degradation of heavy polar OM components into saturated and aromatic hydrocarbons and leading to the production of EOM enriched in saturated and aromatic components; (iii) has no significant impact on the evolution of KCF rocks' porosity at the early oil generation stage, which is controlled more by the amount of effluents filling the interparticle mineral associated porosity than by the composition of EOM.

In preventing the early breaking of low energy bonds, the lower temperature used for the longer duration experiments results in a less pronounced early cracking of OM, resulting in a different timing of gas generation, more gradual throughout the OM particles. This process does not influence the global evolution of the pore volume during maturation. However, it seems to influence the amplitude and the timing of pore alteration/deformation events that occur during gas generation, leading to slightly different pore size distributions and pore volumes, especially in highly oil-prone samples. The impact of the duration-temperature pairs of thermal maturation experiments on the development of KCF mudstones porosity remains, however, limited, suggesting that results from different time-duration experiments and natural samples can be easily compared.

Journal Pre-proof

**Acknowledgments**

Many thanks to Dr. Rémi Champallier and Mrs. Rachel Boscardin for their assistance in the laboratory. Nitrogen adsorption measurements were carried out at the Institut de Science des Matériaux de Mulhouse (IS2M), France. Special thanks go to Mr. Cyril Vaulot for his expert support in nitrogen adsorption measurements. This work was funded by the council of the Region Centre-Val de Loire, France and supported by a grant overseen by the French National Research Agency (ANR) as part of the "Investments d'Avenir" Programme LabEx VOLTAIRE, 10-LABX-0100.

## References

Barrett, E.P., Joyner, L.G., Halenda, P.P., 1951. The Determination of Pore Volume and Area Distributions in Porous Substances. I. Computations from Nitrogen Isotherms. Journal of the American Chemical Society 73, 373–380. https://doi.org/10.1021/ja01145a126

Behar, F., Lewan, M.D., Lorant, F., Vandenbroucke, M., 2003. Comparison of artificial maturation of lignite in hydrous and nonhydrous conditions. Organic Geochemistry 34, 575–600. https://doi.org/10.1016/S0146-6380(02)00241-3

Bernard, S., Horsfield, B., Schulz, H.-M., Wirth, R., Schreiber, A., Sherwood, N., 2012a. Geochemical evolution of organic-rich shales with increasing maturity: A STXM and TEM study of the Posidonia Shale (Lower Toarcian, northern Germany). Marine and Petroleum Geology 31, 70–89. https://doi.org/10.1016/j.marpetgeo.2011.05.010

Bernard, S., Wirth, R., Schreiber, A., Schulz, H.-M., Horsfield, B., 2012b. Formation of nanoporous pyrobitumen residues during maturation of the Barnett Shale (Fort Worth Basin). International Journal of Coal Geology 103, 3–11. https://doi.org/10.1016/j.coal.2012.04.010

Boreham, C.J., Crick, I.H., Powell, T.G., 1988. Alternative calibration of the Methylphenanthrene Index against vitrinite reflectance: Application to maturity measurements on oils and sediments. Organic Geochemistry 12, 289–294. https://doi.org/10.1016/0146-6380(88)90266-5

Boussafir, M., Gelin, F., Lallier-Vergès, E., Derenne, S., Bertrand, P., Largeau, C., 1995a. Electron microscopy and pyrolysis of kerogens from the Kimmeridge Clay Formation, UK: source organisms, preservation processes, and origin of microcycles. Geochimica et Cosmochimica Acta 59, 3731–3747.

Boussafir, M., Lallier-Vergès, E., 1997. Accumulation of organic matter in the Kimmeridge Clay Formation (KCF): an update fossilisation model for marine petroleum source-rocks. Marine and Petroleum Geology 14, 75–83.

Boussafir, M., Lallier-Vergès, E., Bertrand, P., Badaut-Trauth, D., 1995b. SEM and TEM studies on isolated organic matter and rock microfacies from a short-term organic cycle of the Kimmeridge Clay Formation (Yorkshire, GB)., in: Organic Matter Accumulation. Berlin, Heidelberg, pp. 15–30.

Brunauer, S., Emmett, P.H., Teller, E., 1938. Adsorption of Gases in Multimolecular Layers. Journal of the American Chemical Society 60, 309–319. https://doi.org/10.1021/ja01269a023

Cavelan, A., Boussafir, M., Le Milbeau, C., Laggoun-Défarge, F., 2020. Impact of Oil-Prone Sedimentary Organic Matter Quality and Hydrocarbon Generation on Source Rock Porosity: Artificial Thermal Maturation Approach. ACS Omega. https://doi.org/10.1021/acsomega.0c01432

Cavelan, A., Boussafir, M., Le Milbeau, C., Rozenbaum, O., Laggoun-Défarge, F., 2019a. Effect of organic matter composition on source rock porosity during confined anhydrous thermal

maturation: Example of Kimmeridge-clay mudstones. International Journal of Coal Geology 212. https://doi.org/10.1016/j.coal.2019.103236

Cavelan, A., Boussafir, M., Rozenbaum, O., Laggoun-Défarge, F., 2019b. Organic petrography and pore structure characterization of low-mature and gas-mature marine organic-rich mudstones: Insights into porosity controls in gas shale systems. Marine and Petroleum Geology 103, 331–350.

Chalmers, G.R., Bustin, R.M., Power, I.M., 2012. Characterization of gas shale pore systems by porosimetry, pycnometry, surface area, and field emission scanning electron microscopy/transmission electron microscopy image analyses: Examples from the Barnett, Woodford, Haynesville, Marcellus, and Doig units. AAPG Bulletin 96, 1099–1119. https://doi.org/10.1306/10171111052

Chalmers, G.R.L., Bustin, R.M., 2008. Lower Cretaceous gas shales in northeastern British Columbia, Part I: geological controls on methane sorption capacity. Bulletin of Canadian Petroleum Geology 56, 1–21. https://doi.org/10.2113/gscpgbull.56.1.1

Chen, J., Xiao, X., 2014. Evolution of nanoporosity in organic-rich shales during thermal maturation. Fuel 129, 173–181. https://doi.org/10.1016/j.fuel.2014.03.058

Clarkson, C.R., Solano, N., Bustin, R.M., Bustin, A.M.M., Chalmers, G.R.L., He, L., Melnichenko, Y.B., Radliński, A.P., Blach, T.P., 2013. Pore structure characterization of North American shale gas reservoirs using USANS/SANS, gas adsorption, and mercury intrusion. Fuel 103, 606–616. https://doi.org/10.1016/j.fuel.2012.06.119

Curtis, M.E., Cardott, B.J., Sondergeld, C.H., Rai, C.S., 2012. Development of organic porosity in the Woodford Shale with increasing thermal maturity. International Journal of Coal Geology 103, 26–31. https://doi.org/10.1016/j.coal.2012.08.004

Desprairies, A., Bachaoui, M., Ramdani, A., Tribovillard, N., 1995. Clay diagenesis in organic-rich cycles from the Kimmeridge Clay Formation of Yorshire (G.B.): implication for palaeoclimatic interpretations, in: Organic Matter Accumulation. Springer Berlin Heidelberg, Berlin, Heidelberg, pp. 63–91. https://doi.org/10.1007/BFb0117668

DiStefano, V.H., McFarlane, J., Anovitz, L.M., Stack, A.G., Gordon, A.D., Littrell, K.C., Chipera, S.J., Hunt, R.D., Lewis, S.A., Hale, R.E., Perfect, E., 2016. Extraction of organic compounds from representative shales and the effect on porosity. Journal of Natural Gas Science and Engineering 35, 646–660. https://doi.org/10.1016/j.jngse.2016.08.064

Espitalie, J., Deroo, G., Marquis, F., 1985a. Rock-Eval pyrolysis and its applications. Revue De L Institut Francais Du Petrole 40, 563–579.

Espitalie, J., Deroo, G., Marquis, F., 1985b. Rock-Eval pyrolysis and ots application. 2. Revue De L'Institut Francais Du Petrole 40, 755–784.

Furmann, A., Mastalerz, M., Bish, D., Schimmelmann, A., Pedersen, P.K., 2016. Porosity and pore size distribution in mudrocks from the Belle Fourche and Second White Specks Formations in Alberta, Canada. Bulletin 100, 1265–1288. https://doi.org/10.1306/02191615118

Gallois, R.W., 2004. The Kimmeridge Clay: the most intensively studied formation in Britain. Open University Geological Journal 25.

Guo, H., He, R., Jia, W., Peng, P., Lei, Y., Luo, X., Wang, X., Zhang, L., Jiang, C., 2018. Pore characteristics of lacustrine shale within the oil window in the Upper Triassic Yanchang Formation, southeastern Ordos Basin, China. Marine and Petroleum Geology 91, 279–296. https://doi.org/10.1016/j.marpetgeo.2018.01.013

Guo, H., Jia, W., Peng, P., Zeng, J., He, R., 2017. Evolution of organic matter and nanometer-scale pores in an artificially matured shale undergoing two distinct types of pyrolysis: A study of the Yanchang Shale with Type II kerogen. Organic Geochemistry 105, 56–66. https://doi.org/10.1016/j.orggeochem.2017.01.004

Han, H., Pang, P., Li, Z., Shi, P., Guo, C., Liu, Y., Chen, S., Lu, J., Gao, Y., 2019. Controls of organic and inorganic compositions on pore structure of lacustrine shales of Chang 7 member from Triassic Yanchang Formation in the Ordos Basin, China. Marine and Petroleum Geology 100, 270–284. https://doi.org/10.1016/j.marpetgeo.2018.10.038

Han, Y., Horsfield, B., Wirth, R., Mahlstedt, N., Bernard, S., 2017. Oil retention and porosity evolution in organic-rich shales. Bulletin 101, 807–827. https://doi.org/10.1306/09221616069

Herbin, J.P., Fernandez-Martinez, J.L., Geyssant, J.R., Albani, A.El., Deconinck, J.F., Proust, J.N., Colbeaux, J.P., Vidier, J.P., 1995. Sequence stratigraphy of source rocks applied to the study of the Kim meridgian/Tithonian in the north-west European shelf (Dorset/UK, Yorkshire/UK and Boulonnais/France). Marine and Petroleum Geology 12, 177–194. https://doi.org/10.1016/0264-8172(95)92838-N

Hu, H., Zhang, T., Wiggins-Camacho, J.D., Ellis, G.S., Lewan, M.D., Zhang, X., 2015. Experimental investigation of changes in methane adsorption of bitumen-free Woodford Shale with thermal maturation induced by hydrous pyrolysis. Marine and Petroleum Geology 59, 114–128.

Jarvie, D.M., Hill, R.J., Ruble, T.E., Pollastro, R.M., 2007. Unconventional shale-gas systems: The Mississippian Barnett Shale of north-central Texas as one model for thermogenic shale-gas assessment. Bulletin 91, 475–499. https://doi.org/10.1306/12190606068

Juliao, T., Suárez-Ruiz, I., Marquez, R., Ruiz, B., 2015. The role of solid bitumen in the development of porosity in shale oil reservoir rocks of the Upper Cretaceous in Colombia. International Journal of Coal Geology 147–148, 126–144. https://doi.org/10.1016/j.coal.2015.07.001

Katz, B.J., Arango, I., 2018. Organic porosity: A geochemist's view of the current state of understanding. Organic Geochemistry 123, 1–16. https://doi.org/10.1016/j.orggeochem.2018.05.015

Ko, L.T., Loucks, R.G., Zhang, T., Ruppel, S.C., Shao, D., 2016. Pore and pore network evolution of Upper Cretaceous Boquillas (Eagle Ford–equivalent) mudrocks: Results from gold tube pyrolysis experiments. AAPG Bulletin 100, 1693–1722. https://doi.org/10.1306/04151615092

Ko, L.T., Ruppel, S.C., Loucks, R.G., Hackley, P.C., Zhang, T., Shao, D., 2018. Pore-types and pore-network evolution in Upper Devonian-Lower Mississippian Woodford and Mississippian Barnett mudstones: Insights from laboratory thermal maturation and organic petrology. International Journal of Coal Geology 190, 3–28. https://doi.org/10.1016/j.coal.2017.10.001

Kuila, U., McCarty, D.K., Derkowski, A., Fischer, T.B., Topór, T., Prasad, M., 2014. Nano-scale texture and porosity of organic matter and clay minerals in organic-rich mudrocks. Fuel 135, 359–373. https://doi.org/10.1016/j.fuel.2014.06.036

Lafargue, E., Marquis, F., Pillot, D., 1998. Rock-Eval 6 Applications in Hydrocarbon Exploration, Production, and Soil Contamination Studies. Revue de l'Institut Français du Pétrole 53, 421–437. https://doi.org/10.2516/ogst:1998036

Landais, P., 1991. Assessment of coal potential evolution by experimental simulation of natural coalification. Organic Geochemistry 17, 705–710. https://doi.org/10.1016/0146-6380(91)90014-B

Landais, P., Michels, R., Elie, M., 1994. Are time and temperature the only constraints to the simulation of organic matter maturation? Organic Geochemistry 22, 617–630. https://doi.org/10.1016/0146-6380(94)90128-7

Loucks, R.G., Reed, R.M., Ruppel, S.C., Hammes, U., 2012. Spectrum of pore types and networks in mudrocks and a descriptive classification for matrix-related mudrock pores. Bulletin 96, 1071–1098. https://doi.org/10.1306/08171111061

Loucks, R.G., Reed, R.M., Ruppel, S.C., Jarvie, D.M., 2009. Morphology, Genesis, and Distribution of Nanometer-Scale Pores in Siliceous Mudstones of the Mississippian Barnett Shale. Journal of Sedimentary Research 79, 848–861. https://doi.org/10.2110/jsr.2009.092

Mackenzie, A.S., Patience, R.L., Maxwell, J.R., Vandenbroucke, M., Durand, B., 1980. Molecular parameters of maturation in the Toarcian shales, Paris Basin, France—I. Changes in the configurations of acyclic isoprenoid alkanes, steranes and triterpanes. Geochimica et Cosmochimica Acta 44, 1709–1721.

Mastalerz, M., Schimmelmann, A., Drobniak, A., Chen, Y., 2013. Porosity of Devonian and Mississippian New Albany Shale across a maturation gradient: Insights from organic petrology, gas adsorption, and mercury intrusion. AAPG Bulletin 97, 1621–1643. https://doi.org/10.1306/04011312194

Michels, R., Landais, P., Elie, M., Gerard, L., Mansuy, L., 1992. Evaluation of factors influencing the thermal maturation of organic matter during confined pyrolysis experiments. ABSTRACTS OF PAPERS OF THE AMERICAN CHEMICAL SOCIETY 204, 76.

Journal Pre-proof

Michels, R., Landais, P., Torkelson, B.E., Philp, R.P., 1995. Effects of effluents and water pressure on oil generation during confined pyrolysis and high-pressure hydrous pyrolysis. Geochimica et Cosmochimica Acta 59, 1589–1604. https://doi.org/10.1016/0016-7037(95)00065-8

Milliken, K.L., Rudnicki, M., Awwiller, D.N., Zhang, T., 2013. Organic matter-hosted pore system, Marcellus Formation (Devonian), Pennsylvania. Bulletin 97, 177–200. https://doi.org/10.1306/07231212048

Modica, C.J., Lapierre, S.G., 2012. Estimation of kerogen porosity in source rocks as a function of thermal transformation: Example from the Mowry Shale in the Powder River Basin of Wyoming. Bulletin 96, 87–108. https://doi.org/10.1306/04111110201

Pan, L., Xiao, X., Tian, H., Zhou, Q., Chen, J., Li, T., Wei, Q., 2015. A preliminary study on the characterization and controlling factors of porosity and pore structure of the Permian shales in Lower Yangtze region, Eastern China. International Journal of Coal Geology 146, 68–78. https://doi.org/10.1016/j.coal.2015.05.005

Peters, K.E., Walters, C.C., Moldowan, J.M., Peters, K.E., 2007. Biomarkers and isotopes in the environment and human history, 2. ed., reprinted with corrections, digitally printed version 2007. ed, The biomarker guide. Cambridge Univ. Press, Cambridge, UK.

Powell, J.H., 2010. Jurassic sedimentation in the Cleveland Basin: a review. Proceedings of the Yorkshire Geological Society 58, 21–72. https://doi.org/10.1144/pygs.58.1.278

Radke, M., 1988. Application of aromatic compounds as maturity indicators in source rocks and crude oils. Marine and Petroleum Geology 5, 224–236. https://doi.org/10.1016/0264-8172(88)90003-7

Radke, M., Welte, D.H., Willsch, H., 1986. Maturity parameters based on aromatic hydrocarbons: Influence of the organic matter type. Organic Geochemistry 10, 51–63. https://doi.org/10.1016/0146-6380(86)90008-2

Ramanampisoa, L., Disnar, J.R., 1994. Primary control of paleoproduction on organic matter preservation and accumulation in the Kimmeridge rocks of Yorkshire (UK). Organic Geochemistry 21, 1153–1167. https://doi.org/10.1016/0146-6380(94)90160-0

Ramanampisoa, L.R., Radke, M., 1995. Extractable aromatic hydrocarbons in a short-term organic cycle of the Kimmeridge Clay formation, Yorkshire (U.K.): relationship to primary production and thermal maturity. Organic Geochemistry 23, 803–817. https://doi.org/10.1016/0146-6380(95)80002-9

Rawson, P.F., Riley, L.A., 1982. Latest Jurassic - Early Cretaceous Events and the "Late Cimmerian Unconformity" in North Sea Area. AAPG Bulletin, AAPG Bulletin 66, 2628–2648.

Schmitt, M., Fernandes, C.P., da Cunha Neto, J.A.B., Wolf, F.G., dos Santos, V.S.S., 2013. Characterization of pore systems in seal rocks using Nitrogen Gas Adsorption combined with Mercury Injection Capillary Pressure techniques. Marine and Petroleum Geology 39, 138–149.

Seifert, W.R., Moldowan, J.M., 1981. Paleoreconstruction by biological markers. Geochimica et Cosmochimica Acta 45, 783–794.

Sing, K.S., 1985. Reporting physisorption data for gas/solid systems with special reference to the determination of surface area and porosity (Recommendations 1984). Pure and applied chemistry 57, 603–619.

Song, L., Martin, K., Carr, T.R., Ghahfarokhi, P.K., 2019. Porosity and storage capacity of Middle Devonian shale: A function of thermal maturity, total organic carbon, and clay content. Fuel 241, 1036–1044. https://doi.org/10.1016/j.fuel.2018.12.106

Tissot, Welte, D.H., 1984. Petroleum formation and occurence, 2. rev. and enl. ed. ed. Springer, Berlin, Heidelberg [usw.].

Wang, X., Jiang, Z., Jiang, S., Chang, J., Li, X., Wang, Xin, Zhu, L., 2020. Pore Evolution and Formation Mechanism of Organic-Rich Shales in the Whole Process of Hydrocarbon Generation: Study of Artificial and Natural Shale Samples. Energy Fuels 34, 332–347. https://doi.org/10.1021/acs.energyfuels.9b03789

Wang, Y., Liu, L., Hu, Q., Hao, L., Wang, X., Sheng, Y., 2020. Nanoscale Pore Network Evolution of Xiamaling Marine Shale during Organic Matter Maturation by Hydrous Pyrolysis. Energy Fuels 34, 1548–1563. https://doi.org/10.1021/acs.energyfuels.9b03686

Journal Pre-proof

Wang, Y., Liu, L., Zheng, S., Luo, Z., Sheng, Y., Wang, X., 2019. Full-scale pore structure and its controlling factors of the Wufeng-Longmaxi shale, southern Sichuan Basin, China: Implications for pore evolution of highly overmature marine shale. Journal of Natural Gas Science and Engineering 67, 134–146. https://doi.org/10.1016/j.jngse.2019.04.020

Wood, D.A., 1988. Relationships between thermal maturity indices calculated using Arrhenius equation and Lopatin method: implications for petroleum exploration. Assoc. Pet. Geol. Bull. 72, 115–134.

Wu, S., Yang, Z., Zhai, X., Cui, Jingwei, Bai, L., Pan, S., Cui, Jinggang, 2019. An experimental study of organic matter, minerals and porosity evolution in shales within high-temperature and high-pressure constraints. Marine and Petroleum Geology 102, 377–390. https://doi.org/10.1016/j.marpetgeo.2018.12.014

Zhang, T., Ellis, G.S., Ruppel, S.C., Milliken, K.L., Lewan, M.D., Sun, X., 2013. Effect of organic matter properties, clay mineral type and thermal maturity on gas adsorption in organic-rich shale systems. Presented at the Unconventional Resources Technology Conference, Society of Exploration Geophysicists, American Association of Petroleum Geologists, Society of Petroleum Engineers, pp. 1996–2001.

## Appendix 1

Calculation of biomarker ratios

- MDBT: methyldibenzothiophene ratio = 4-MDBT/1-MDBT (Radke, 1988).
- $R_{MDBT}$ (%) = 0.40 + 0.30*MDR – 0.094*$MDR^2$ + 0.011*$MDR^3$ (Radke, 1988).
- DPR: dimethylphenanthrene ratio = (2,6-DMP + 2,7-DMP + 3,5-DMP) / (1,3-DMP + 1,6-DMP + 2,5-DMP + 2,9-DMP + 2,10-DMP + 3,9-DMP + 3,10-DMP) (Radke, 1988).
- $R_{DPR}$ (%) = 1.50 + 1.34*$\log_{10}$ DPR (Radke, 1988).
- MPI-1: methylphenanthrene index = 1.5 * (2-MP + 3MP) / (Ph + 1-MP + 9-MP) (Radke et al., 1986).
- $R_{MPI-1}$ (%): for Ro ≤ 1.4%, Ro = 0.7*MPI-1 + 0.22 (Boreham et al., 1988). For Ro ≥ 1.4%, Rc =-0.55*MPI-1 + 3.0 (Boreham et al., 1988).
- Mean calculated vitrinite reflectance, Rc (%) = ($R_{MDBT}$+ $R_{DPR}$+ $R_{MPI-1}$)/3.

Journal Pre-proof

Journal Pre-proof

**Highlights**

- Long and short-duration thermal maturation experiments are compared.
- Longer duration experiments enhance the degradation of polar organic components.
- Longer duration experiments exhibit slightly different gas concentrations.
- Duration-temperature pairs do not greatly influence the evolution trend of porosity.
- Duration-temperature pairs influence pore size distributions and pore volumes.

Journal Pre-proof

Journal Pre-proof

**Declaration of interests**

☒ The authors declare that they have no known competing financial interests or personal relationships that could have appeared to influence the work reported in this paper.

☐The authors declare the following financial interests/personal relationships which may be considered as potential competing interests:

Journal Pre-proof